HHS Public Access

Author manuscript

J Magn Reson Imaging. Author manuscript; available in PMC 2018 June 01.

Published in final edited form as:

J Magn Reson Imaging. 2017 June ; 45(6): 1712–1722. doi:10.1002/jmri.25507.

Knee Imaging: Rapid Three-Dimensional Fast Spin-Echo Using Compressed Sensing

Richard Kijowski, M.D.[1], **Humberto Rosas, M.D.**[1], **Alexey Samsonov, Ph.D.**[1], **Kevin King, Ph.D.**[2], **Rob Peters, Ph.D.**[2], and **Fang Liu, Ph.D.**[1,3]

[1]Department of Radiology, University of Wisconsin School of Medicine and Public Health, Madison, Wisconsin

[2]Global Applied Science Lab, General Electric Healthcare, Waukesha, Wisconsin

Abstract

Introduction—To investigate the feasibility of using compressed sensing (CS) to accelerate three-dimensional fast spin-echo (3D-FSE) imaging of the knee.

Methods—A 3D-FSE sequence was performed at 3T with CS (CUBE-CS with 3:16 minute scan time) and without CS (CUBE with 4:44 minute scan time) twice on the knees of 10 healthy volunteers to assess signal-to-noise ratio (SNR) using the addition-subtraction method and once on the knees of 50 symptomatic patients to assess diagnostic performance. SNR of cartilage, muscle, synovial fluid, and bone marrow on CUBE and CUBE-CS images were measured in the 10 healthy volunteers. The CUBE and CUBE-CS sequences of all 50 symptomatic patients were independently reviewed twice by two musculoskeletal radiologists. The radiologists used CUBE and CUBE-CS during each individual review to determine the presence or absence of knee joint pathology. Student t-tests were used to compare SNR values between sequences, while kappa statistic was used to determine agreement between sequences for detecting knee joint pathology. Sensitivity and specificity of Cube and Cube-CS for detecting knee joint pathology was also calculated in the 18 symptomatic patients who underwent subsequent arthroscopic knee surgery.

Results—CUBE and CUBE-CS had similar SNR (p=0.15-0.67) of cartilage, muscle, synovial fluid, and bone marrow. There was near perfect to perfect agreement between CUBE and CUBE-CS for both radiologists for detecting cartilage and bone marrow edema lesions, medial and lateral meniscus tears, anterior cruciate ligament tears, effusions, and intra-articular bodies. Cube and Cube-CS had similar sensitivity (75.0%-100%) and specificity (87.5%-100%) for detecting 60 cartilage lesions, 20 meniscus tears, four anterior cruciate ligament tears, and four intra-articular bodies confirmed at surgery.

Conclusions—CS provided a 30% reduction in scan time for 3D-FSE imaging of the knee without a corresponding decrease in SNR or diagnostic performance.

Keywords

Three-Dimensional; Fast Spin-Echo; Compressed Sensing; Knee

[3]Corresponding Author: Fang Liu, Ph.D., Department of Radiology, 1111 Highland Avenue, Madison, Wisconsin 53705-2275, Phone: 608-265-3247, FAX: 608-263-5112, fliu37@wisc.edu.

Introduction

Current musculoskeletal magnetic resonance imaging (MRI) protocols typically consist of two-dimensional fast spin-echo (2D-FSE) sequences acquired in multiple planes. Three-dimensional fast spin-echo (3D-FSE) sequences are now commercially available on most MRI vendor platforms. 3D-FSE sequences can acquire thin continuous slices through joints which can be reformatted in any orientation, thereby eliminating the need to repeat sequences with identical tissue contrast in multiple planes (1). The use of 3D-FSE sequences in clinical practice could significantly decrease MRI examination times which would improve patient comfort and increase the clinical efficiency of the MRI scanner.

Multiple studies have shown that 3D-FSE sequences provide similar diagnostic performance as 2D-FSE sequences for evaluating the knee joint (2-6). However, 3D-FSE sequences are currently limited by their long scan times needed to achieve high isotropic resolution. 3D-FSE sequences typically use parallel imaging to reduce scan time at the expense of decreased signal-to-noise ratio (SNR). Scan time reduction has also been achieved by using low isotropic resolutions and long echo train lengths which result in image blurring (2-4) or by using anisotropic voxel sizes which reduce the quality of multi-planar reformat images (5,6).

Compressed sensing (CS) is an alternative method which could reduce the scan time of 3D-FSE sequences by acquiring less image data through k-space undersampling (7,8). CS has been successfully used to accelerate vascular, cardiac, body, pediatric, and brain imaging, but applications of this technique in musculoskeletal imaging remain limited due to the need to maintain high image quality to detect subtle pathology in small joint structures (9). This study was performed to investigate the feasibility of using CS to accelerate 3D-FSE imaging of the knee. In particular, 3D-FSE sequences with and without CS were compared to determine if CS could reduce scan time without decreasing image quality or diagnostic performance.

Methods

Study Group

The study was performed in compliance with Health Insurance Portability and Accountability Act (HIPPA) regulations and with approval from our Institutional Review Board. All subjects signed written informed consent prior to their participation in the study. The study group consisted of 10 healthy volunteers who had no history of prior knee pain, trauma, or surgery and 50 symptomatic patients who were undergoing a clinical MRI examination of the knee at our institution.

MRI Examination

An intermediate-weighted 3D-FSE sequence (CUBE, GE Healthcare, Waukesha, WI) was performed with CS (CUBE-CS) and without CS (CUBE) on the knees of 10 healthy volunteers and 50 symptomatic patients using the same 3T scanner (Discovery MR750, GE Healthcare, Waukesha, WI) and 8-channel phased-array extremity coil (Precision Eight

TX/TR High Resolution Knee Array, InVivo, Orlando, Florida). To assess SNR performance, CUBE and CUBE-CS were performed twice on the same knees of the 10 healthy volunteers with the subjects taken off the MRI table and then repositioned between repeat scans. CUBE and CUBE-CS were acquired using a 1500ms repetition time, 20ms effective echo time, 90° flip angle, 16cm field of view, 320 × 320 matrix, 1.0mm slice thickness, 0.5mm × 0.5mm × 1.0mm voxel size, 2.0 parallel imaging reconstruction (Autocalibrating Reconstruction for Cartesian sampling (ARC), GE Healthcare, Waukesha, WI) acceleration factor in the phase and slice directions (10), 40 echo train length, one excitation, and fat-saturation using a GE Healthcare product frequency selective method.

The CUBE-CS reconstruction was performed using a previously described method combining CS and parallel imaging (11). The CS k-space undersampling pattern was first generated using the undersampling needed for ARC parallel imaging and then randomly undersampled outside of a small area near the center of k-space. The k-space data was subsampled on the uniform ARC grid. The samples randomly missing on the grid were then restored by minimizing the total variation of each separate coil image using a conjugate gradient minimizer with 10 iterations while maintaining consistency with acquired k-space data. The consistency of acquired data was maintained without need for a regularization parameter by substituting the acquired k-space data back into the new k-space after each iteration. The resulting k-space data was combined with the original sampled k-space data to restore the missing ARC signal area. After ARC processing, the final k-space was fully sampled and sum-of-squares coil combination was performed (11). CUBE-CS was acquired using a 1.5 k-space undersampling factor which corresponded to 63.3% undersampled image data. The scan times of CUBE and CUBE-CS were 4:44 minutes and 3:16 minutes respectively.

Quantitative Image Analysis

CUBE and CUBE-CS performed twice on the knees of the 10 healthy volunteers were used to quantitatively compare SNR performance in multiple musculoskeletal tissues. Addition and subtraction images for CUBE and CUBE-CS were created. The SNR of cartilage, muscle, synovial fluid, and bone marrow and the contrast-to-noise ratio (CNR) between cartilage and synovial fluid, cartilage and bone marrow, cartilage and muscle, and synovial fluid and muscle were calculated using a previously described double acquisition method (12). Regions of interests (ROIs) containing 100 pixels for cartilage and synovial fluid, 200 pixels for bone marrow, and 400 pixels for muscle were placed at identical locations on the addition and subtraction images for CUBE and CUBE-CS. Signal (S) was defined as the average signal within the ROIs, while noise standard deviation (σ) was defined based on the standard deviation of the signal within the ROIs on the subtraction images (12). SNR and CNR were calculated using the equations:

$$\mathrm{SNR}=\frac{S}{\sigma} \quad (1)$$

$$\mathrm{CNR}=\frac{|S_{\mathrm{Tissue1}}-S_{\mathrm{Tissue2}}|}{\sigma} \quad (2)$$

A retrospective image based homomorphic approach was also used to estimate the spatially variant noise behavior for CUBE and CUBE-CS in the 10 healthy volunteers (13). The voxel-wise noise standard deviation was calculated for all image voxels by a homomorphic separation of the stationary noise term and a low frequency location-dependent variance of noise as:

$$\hat{\sigma}(\mathrm{x})=\sqrt{2}e^{\mathrm{LPF}\{\log|\mathrm{I(x)}-\mathrm{E\{I(x)\}}|\}+\gamma/2} \quad (3)$$

where $\hat{\sigma}$ is an estimator for noise standard deviation, I(x) is the image intensity, x is the voxel location, LPG{*} and E{*} are spatial low pass filter and an estimator for local mean value respectively, and γ is the Euler-Mascheroni constant. The estimated noise standard deviation map was generated for both CUBE and CUBE-CS. The noise amplification (NA) factor, which is similar to *g*-factor (14), was calculated as

$$\mathrm{NA}=\frac{\hat{\sigma}_{\mathrm{CUBE}}}{\hat{\sigma}_{\mathrm{CUBE-CS}}\sqrt{\mathrm{R}}} \quad (4)$$

where R is the undersampling factor. The mean NA factor for the entire knee joint was then calculated for each subject as an indicator of overall noise amplification.

Qualitative Image Analysis

CUBE and CUBE-CS performed on the 50 symptomatic patients were used to compare qualitative measures of image quality and diagnostic performance for detecting knee joint pathology. CUBE and CUBE-CS were independently evaluated twice in random order by two fellowship-trained musculoskeletal radiologists with 11 and 13 years of clinical experience. To prevent recall bias, the radiologists evaluated the sequences at separate sittings at least one month apart. During the first review, the radiologists used CUBE with multi-planar reformat images to detect the presence or absence of knee joint pathology including cartilage and bone marrow edema lesions on each articular surface, medial and lateral meniscus tears, anterior cruciate ligament tears, effusions defined as a grade of 1 or higher using the Whole-Organ MRI Score (WORMS) system (15), and intra-articular bodies. Posterior cruciate ligament tears, medial and lateral collateral ligament tears, and patellar and quadriceps tendon injuries were not assessed since these abnormalities were not common in our patient population. During the second review, the radiologists used CUBE-CS with multi-planar reformat images to detect the same knee joint pathology. The radiologists also independently performed a side-by-side comparison of CUBE and CUBE-CS in a third review to assess various qualitative features of image quality including SNR,

tissue contrast, clarity of cartilage, meniscus, tendon, and muscle, presence of image artifact, and conspicuity of knee joint pathology. The radiologists used a five category grading system (CUBE much better than CUBE-CS, CUBE slightly better than CUBE-CS, CUBE and CUBE-CS identical, CUBE-CS slightly better than CUBE, and CUBE-CS sequence much better than CUBE) to compare image quality of the two sequences.

Arthroscopic Knee Surgery

Eighteen of the 50 symptomatic patients in the study group underwent subsequent arthroscopic knee surgery at our institution within four months (time range of 10 days to 101 days with an average time of 35 days and a standard deviation of 24 days) of their MRI examination. All arthroscopic knee surgeries were performed by one of three experienced orthopedic surgeons at our institution who specialized in sports medicine and who had between 15 and 25 years of clinical experience. The orthopedic surgeons were aware of the official interpretations of the MRI examinations of all patients at the time of arthroscopy which was made using the conventional 2D-FSE sequences as mandated by our Internal Review Board. The surgeons documented in their operative reports the presence or absence of cartilage lesions on each articular surface, medial and lateral meniscus tears, anterior cruciate ligament tears, and intra-articular bodies at arthroscopy. The operative reports of all patients were retrospectively reviewed to determine the presence or absence of knee joint pathology.

Phantom Experiments

Cube and Cube-CS were performed on a phantom set made of four tubes with gelatin gel (Sigma-Aldrich, Co. LLC., St. Louis, MO) at different percent weight varying from 20% to 50% with a T2 relaxation time range between 28ms and 156ms and a low resolution phantom filled with 0.18mmol/L ferumoxides solution (Feridex I.V., Advanced Magnetics, Inc., Cambridge, MA) with cylinders of diameters varying from 2mm to 12mm using the same 3T scanner (Discovery MR750, GE Healthcare, Waukesha, WI) and 8-channel phased-array extremity coil (Precision Eight TX/TR High Resolution Knee Array, InVivo, Orlando, Florida). CUBE and CUBE-CS were also performed on the American College of Radiology 0.9mm high resolution MRI phantom (American College of Radiology, Reston, VA) using the same 3T scanner (Discovery MR750, GE Healthcare, Waukesha, WI) and 16-channel wrap coil (GEM Flex, GE Healthcare, Waukesha, WI). The 8-channel extremity coil could not be used to image the American College of Radiology MRI phantom due to its large size. The phantom experiments were performed using the same CUBE and CUBE-CS imaging parameters as described for human subjects.

Statistical Analysis

Statistical analysis was performed using the R programming environment (R Foundation of Statistical Imaging; Vienna, Austria; Version 2.3.1; 2006; http:/www.R-project.org). Statistical significance was defined as a p-value less than 0.05 with the Holm-Bonferroni correction method used to adjust p-values for multiple comparisons between sequences (16). Student t-tests were used to compare SNR and CNR values between CUBE and CUBE-CS. Kappa statistics were used to determine agreement between CUBE and CUBE-CS for detecting knee joint pathology for each radiologist. Kappa statistics was also used to

determine agreement between the two radiologists for detecting knee joint pathology when using CUBE and CUBE-CS. Agreement was assessed according to the recommendations of Landis and Koch (17). Chi-squared tests were used to compare the proportions of patients graded CUBE slightly greater than CUBE-CS and the proportion of patients graded CUBE-CS slightly greater than CUBE for all qualitative measures of image quality for each radiologist. Using the surgical findings as the reference standard, the sensitivity and specificity with 95% confidence intervals of CUBE and CUBE-CS for detecting all cartilage lesions combined, anterior cruciate ligament tears, medial and lateral meniscus tears combined, and intra-articular bodies were calculated.

Results

The 10 healthy volunteers who underwent repeat CUBE and CUBE-CS scans to assess SNR and CNR included 6 males with an average age of 29 years and 4 females with an average age of 25 years. There was no statistically significant difference (p=0.15-0.67) between CUBE and CUBE-CS in the SNR of cartilage, muscle, synovial fluid, and bone marrow (Figure 1a). In addition, there was no statistically significant difference (p=0.38-0.80) between CUBE and CUBE-CS in the CNR between cartilage and synovial fluid, cartilage and bone marrow, cartilage and muscle, and synovial fluid and muscle (Figure 1b).

Figure 2 shows examples of the estimated low frequency noise standard deviation maps for two healthy volunteers (Figure 2a). The voxel-wise NA factor maps showed a non-uniform noise amplification behavior across the entire knee joint when using CS (Figure 2b). The histogram of the NA factor distribution varied between different subjects but had a mean value close to 1 in all individuals (Figure 2c). The mean value of the NA factor distribution for all 10 healthy volunteers was 0.91 with a standard deviation of 0.12 indicating no noise amplification.

There was less than 1% difference in the signal intensities of the gelatin gel phantoms on the CUBE and CUBE-CS images. There was image blurring on the CUBE-CS images for the low resolution phantom, but this did not result in a visible reduction in spatial resolution for cylinders with diameters varying from 2mm to 12mm (Figure 3). There was more extensive image blurring on the CUBE-CS images for the 0.9mm high resolution phantom which resulted in a visible reduction in spatial resolution with apparent decrease in the distance between the dots in the phantoms. The decrease in spatial resolution was more prominent on the low contrast phantom than the high contrast phantom (Figure 4).

The 50 symptomatic patients who were evaluated with CUBE and CUBE-CS included 27 males with an average age of 38 years and 23 females with an average age of 36 years. There was perfect agreement between CUBE and CUBE-CS for both radiologists for detecting medial and lateral meniscus tears, anterior cruciate ligament tears, effusions, and intra-articular bodies and near perfect agreement for detecting cartilage and bone marrow edema lesions (Table 1). There was perfect agreement between radiologists for both CUBE and CUBE-CS for detecting lateral meniscus tears and anterior cruciate ligament tears and near perfect agreement for detecting cartilage and bone marrow edema lesions, medial

meniscus tears, effusions, and intra-articular bodies (Table 2). The vast majority of knee joint pathology appeared similar on CUBE and CUBE-CS images (Figure 5).

The 18 symptomatic patients who were evaluated with CUBE and CUBE-CS and underwent subsequent arthroscopic knee surgery included 10 males with an average age of 43 years and 8 females with an average age of 41 years. There were 60 cartilage lesions, 20 meniscus tears, four anterior cruciate ligament tears, and four intra-articular bodies confirmed at surgery. For radiologist 1, the sensitivity and specificity with 95% confidence intervals for detecting cartilage lesions was 88.3% (77.4%-95.2%) and 87.5% (74.8%-95.3%) respectively for CUBE and 81.7% (69.6%-90.5%) and 91.7% (80.0%-97.7%) respectively for CUBE-CS. For radiologist 2, the sensitivity and specificity with 95% confidence intervals for detecting cartilage lesions was 75.0% (62.1%-85.3%) and 91.7% (80.0%-97.7%) respectively for CUBE and 75.0% (62.1%-85.3%) and 93.8% (82.8%-98.7%) respectively for CUBE-CS. For both radiologists 1 and 2, the sensitivity and specificity with 95% confidence intervals was 95% (75.1%-99.9%) and 100% (79.4%-100%) respectively for detecting meniscus tears, 100% (39.8%-100%) and 100% (76.9%-100%) respectively for detecting anterior cruciate ligament tears, and 100% (39.8%-100%) and 100% (76.8%-100%) respectively for detecting intra-articular bodies for both CUBE and CUBE-CS.

Table 3 shows a comparison of qualitative measures of image quality between CUBE and CUBE-CS. For most patients, both radiologists graded CUBE and CUBE-CS identical for all qualitative measures of image quality. However, there was a significant increase ($p<0.05$) for both radiologists in the proportion of patients that were graded CUBE slightly better than CUBE-CS for clarity of cartilage, meniscus, tendon, and muscle and conspicuity of knee joint pathology. There was no significant increase ($p=0.15$-0.56) in the proportion of patients that were graded CUBE slightly better than CUBE-CS for SNR and tissue contrast. All cases in which CUBE was graded slightly better than CUBE-CS for conspicuity of knee joint pathology were due to improved visualization of superficial cartilage lesions on CUBE images due to decreased image blurring (Figure 6). Artifacts were identified on CUBE-CS images in four patients for radiologist 1 and two patients for radiologist 2 which consisted of linear, vertically-oriented structured noise within the bone marrow of the femur and tibia in all individuals.

Discussion

Our study has demonstrated the feasibility of using CS to accelerate 3D-FSE imaging of the knee. Applications of CS in musculoskeletal imaging remain limited (9). Madelin et al. (18) and Zhou et al. (19) demonstrated the ability of CS to accelerate quantitative sodium and T1-rho imaging of articular cartilage without reducing the accuracy of parameter estimation. Pandit et al. (11) utilized the same combined CS and parallel imaging acquisition and reconstruction algorithm as used in our study to reduce scan time of quantitative T1-rho cartilage imaging by 25% while maintaining similar parameter estimations. Vasanawala et al. (20) used a three-dimensional gradient-recall echo acquired in the steady-state (GRASS) sequence with CS for evaluating the articular cartilage of the knee joint in pediatric patients, while Worters et al. (21) used CS to reduce scan time for metal reduction multi-spectral

imaging of the spine. Our study used CS to accelerate intermediate-weighted 3D-FSE imaging which provides highly versatile tissue contrast that can be used to evaluate all knee joint structures including cartilage, bone, meniscus, tendon, ligament, and synovium.

Our study demonstrated that CUBE-CS could reduce scan time by 30% without a corresponding decrease in SNR. Few previous studies have quantitatively compared SNR of sequences performed with and without CS due to the difficulty in accurately measuring noise behavior (22,23). The spatially variant noise behavior when combining CS and parallel imaging reconstruction is complex and is influenced by multiple factors including coil profile and layout, k-space undersampling strategy, image sparsity properties, selection of the CS regularization term, and actual implementation of the CS regularization when reconstructing the data. More rigorous methods can be performed by acquiring a large number of acquisitions and calculating noise statistics in the temporal dimension, but these techniques require extremely long scan times which are not feasible for *in-vivo* knee imaging (12,24). In our study, noise behavior was measured using a double acquisition method which has been proposed as an effective way of measuring spatially variant noise (12,25), and our results showed no significant difference in SNR between CUBE and CUBE-CS. We also calculated voxel-wise NA factor maps which confirmed that there was no substantial noise amplification when using CUBE-CS. However, our results cannot be extrapolated to other sequences using CS since the SNR measurements only pertain to the CS and parallel imaging reconstruction parameters used in our study (26,27).

3D-FSE sequences such as CUBE utilize variable flip angles for the refocusing radiofrequency pulses to allow the use of long echo train lengths to reduce scan time and provide high resolution and large volume coverage without excessive image blurring. The use of CS k-space undersampling with variable flip angle 3D-FSE imaging may potentially influence which echoes are assigned to the center of k-space and may thereby alter tissue contrast. However, our study showed only small differences in the signal intensities of gelatin gel phantoms with varying T2 relaxation times on CUBE and CUBE-CS images and no significant differences in tissue contrast between CUBE and CUBE-CS on both quantitative and qualitative analysis of the knee joint in human subjects. This is likely due to the fact that the CS reconstruction algorithm used in our study undersampled the higher frequency periphery of k-space while leaving the central low frequency k-space region, which is primarily responsible for tissue contrast, fully sampled. (11). Nevertheless, additional studies are needed to investigate potential alterations in tissue contrast when using CS to accelerate 3D-FSE imaging.

Our study found that CUBE-CS had significantly decreased clarity of cartilage, meniscus, tendon, and muscle and significantly decreased conspicuity of knee joint pathology when compared to CUBE which was primarily due to greater image blurring. The increased image blurring of CS was clearly documented in our phantom experiments and was most prominent when using CUBE-CS to image the high resolution, low contrast phantom. Vasanawala et al. (20) compared GRASS sequences with and without CS for evaluating the pediatric knee joint and found higher image quality and better delineation of anatomic detail for GRASS-CS. However, their study used parallel imaging acceleration factors that were much higher than those used in our study which resulted in extremely noisy images when

not using CS reconstruction. Increased image blurring with CS has been reported by Sharma et al. (28) who used CS to accelerate T2-weighted 2D-FSE imaging of the brain and Worters et al. (21) who used CS to accelerate metal reduction multi-spectral imaging of the spine. The increased image blurring is most likely the result of acquiring a higher proportion of echoes in the central k-space region than in the periphery of k-space where the high spatial frequency information is responsible for image sharpness and detail. CS reconstruction also has a denoising effect which may further increase image blurring as noise can make an image appear sharper (21,29).

Our study found no differences in diagnostic performance between CUBE and CUBE-CS for detecting knee joint pathology although the greater image blurring of CUBE-CS did decrease the conspicuity of superficial cartilage lesions. The greater imaging blurring of CUBE-CS is somewhat concerning as CUBE without CS has been already shown to have increased image blurring when compared to 2D-FSE sequences typically used for joint evaluation (30-32). One application of CS could be to reduce the scan time of current CUBE sequences. However, CS could also be utilized to acquire better quality CUBE images by allowing the use of higher isotropic resolutions and decreased echo train lengths without a resultant increase in scan time. Additional studies are needed to determine the best combination of CS and parallel imaging acceleration, spatial resolution, and echo train length for CUBE imaging to minimize imaging blurring while maintaining short scan times.

Our study has several limitations. One limitation was the inability to blind radiologists to the sequences they were using to evaluate the knee joint as CUBE and CUBE-CS headings were placed on all reconstructed images to allow differentiation between the sequences. In addition, our study was performed to validate a prototype CUBE-CS sequence whose imaging parameters were selected by MRI scientists at GE Healthcare. Finally, our study did not compare CUBE and CUBE-CS with 2D-FSE sequences for evaluating knee joint pathology. However, the CUBE and CUBE-CS sequences used in our study had anisotropic voxel volumes to minimize scan time so that both sequences could be added to the clinical MRI examinations. In our opinion, it would be unfair to compare CUBE and CUBE-CS to the 2D-FSE sequences in the routine MRI protocol in our patient population due to the fact that the anisotropic resolution of the 3D-FSE sequences degraded the quality of multi-planar reformat images.

In conclusion, our study has shown that CS can provide a 30% reduction in scan time for 3D-FSE imaging of the knee without a corresponding decrease in SNR or diagnostic performance. However, the use of CS resulted in greater image blurring which was clearly documented in our phantom experiments and was especially prominent when visualizing low contrast structures. The increased image blurring resulted in significantly decreased clarity of cartilage, meniscus, tendon, and muscle and significantly decreased conspicuity of subtle knee joint pathology such as superficial cartilage lesions. Additional studies with surgical correlation are needed to compare the diagnostic performance of optimized isotropic resolution CUBE-CS sequences with 2D-FSE sequences for providing comprehensive joint assessment in symptomatic patients to further investigate the effects of increased image blurring due to CS acceleration on the detection of knee joint pathology.

Acknowledgments

Grant Support: Research Support Provided by National Institute of Arthritis and Musculoskeletal and Skin Disease Grant R01-AR068373-01

References

1. Gold GE, Busse RF, Beehler C, et al. Isotropic MRI of the knee with 3D fast spin-echo extended echo-train acquisition (XETA): initial experience. AJR American journal of roentgenology. 2007; 188(5):1287–1293. [PubMed: 17449772]
2. Kijowski R, Davis KW, Woods MA, et al. Knee joint: comprehensive assessment with 3D isotropic resolution fast spin-echo MR imaging--diagnostic performance compared with that of conventional MR imaging at 3.0 T. Radiology. 2009; 252(2):486–495. [PubMed: 19703886]
3. Subhas N, Kao A, Freire M, Polster JM, Obuchowski NA, Winalski CS. MRI of the knee ligaments and menisci: comparison of isotropic-resolution 3D and conventional 2D fast spin-echo sequences at 3 T. AJR American journal of roentgenology. 2011; 197(2):442–450. [PubMed: 21785092]
4. Kudo H, Inaoka T, Kitamura N, et al. Clinical value of routine use of thin-section 3D MRI using 3D FSE sequences with a variable flip angle technique for internal derangements of the knee joint at 3T. Magnetic resonance imaging. 2013; 31(8):1309–1317. [PubMed: 23684241]
5. Jung JY, Yoon YC, Kwon JW, Ahn JH, Choe BK. Diagnosis of internal derangement of the knee at 3.0-T MR imaging: 3D isotropic intermediate-weighted versus 2D sequences. Radiology. 2009; 253(3):780–787. [PubMed: 19789228]
6. Ai T, Zhang W, Priddy NK, Li X. Diagnostic performance of CUBE MRI sequences of the knee compared with conventional MRI. Clinical radiology. 2012; 67(12):e58–63. [PubMed: 22974569]
7. Lustig M, Donoho D, Pauly JM. Sparse MRI: The application of compressed sensing for rapid MR imaging. Magnetic resonance in medicine : official journal of the Society of Magnetic Resonance in Medicine / Society of Magnetic Resonance in Medicine. 2007; 58(6):1182–1195.
8. Geethanath S, Reddy R, Konar AS, et al. Compressed sensing MRI: a review. Crit Rev Biomed Eng. 2013; 41(3):183–204. [PubMed: 24579643]
9. Jaspan ON, Fleysher R, Lipton ML. Compressed sensing MRI: a review of the clinical literature. The British journal of radiology. 2015; 88(1056):20150487. [PubMed: 26402216]
10. Beatty, PJ., Brau, AC., Chang, S., et al. Proc Intl Soc Mag Reson Med. Vol. 1749. Berlin, Germany: 2007. A Method for Autocalibrating 2-D Accelerated Volumetric Parallel Imaging with Clinically Practical Reconstruction Times. abstract 310
11. Pandit P, Rivoire J, King K, Li X. Accelerated T1rho acquisition for knee cartilage quantification using compressed sensing and data-driven parallel imaging: A feasibility study. Magnetic resonance in medicine : official journal of the Society of Magnetic Resonance in Medicine / Society of Magnetic Resonance in Medicine. 2016; 75(3):1256–1261.
12. Reeder SB, Wintersperger BJ, Dietrich O, et al. Practical approaches to the evaluation of signal-to-noise ratio performance with parallel imaging: application with cardiac imaging and a 32-channel cardiac coil. Magnetic resonance in medicine : official journal of the Society of Magnetic Resonance in Medicine / Society of Magnetic Resonance in Medicine. 2005; 54(3):748–754.
13. Aja-Fernandez S, Pieciak T, Vegas-Sanchez-Ferrero G. Spatially variant noise estimation in MRI: a homomorphic approach. Med Image Anal. 2015; 20(1):184–197. [PubMed: 25499191]
14. Pruessmann KP, Weiger M, Scheidegger MB, Boesiger P. SENSE: sensitivity encoding for fast MRI. Magnetic resonance in medicine : official journal of the Society of Magnetic Resonance in Medicine / Society of Magnetic Resonance in Medicine. 1999; 42(5):952–962.
15. Peterfy CG, Guermazi A, Zaim S, et al. Whole-Organ Magnetic Resonance Imaging Score (WORMS) of the knee in osteoarthritis. Osteoarthritis and cartilage / OARS, Osteoarthritis Research Society. 2004; 12(3):177–190.
16. Holm S. A Simple Sequentially Rejective Multiple Test Procedure. Scand J Stat. 1979; 6(2):65–70.
17. Landis JR, Koch GG. The measurement of observer agreement for categorical data. Biometrics. 1977; 33(1):159–174. [PubMed: 843571]

18. Madelin G, Chang G, Otazo R, Jerschow A, Regatte RR. Compressed sensing sodium MRI of cartilage at 7T: preliminary study. Journal of magnetic resonance. 2012; 214(1):360–365. [PubMed: 22204825]
19. Zhou Y, Pandit P, Pedoia V, et al. Accelerating t1rho cartilage imaging using compressed sensing with iterative locally adapted support detection and JSENSE. Magnetic resonance in medicine : official journal of the Society of Magnetic Resonance in Medicine / Society of Magnetic Resonance in Medicine. 2016; 75(4):1617–1629.
20. Vasanawala SS, Alley MT, Hargreaves BA, Barth RA, Pauly JM, Lustig M. Improved pediatric MR imaging with compressed sensing. Radiology. 2010; 256(2):607–616. [PubMed: 20529991]
21. Worters PW, Sung K, Stevens KJ, Koch KM, Hargreaves BA. Compressed-sensing multispectral imaging of the postoperative spine. Journal of magnetic resonance imaging : JMRI. 2013; 37(1): 243–248. [PubMed: 22791572]
22. Ding Y, Ying L, Zhang N, Liang D. Noise behavior of MR brain reconstructions using compressed sensing. Conf Proc IEEE Eng Med Biol Soc. 2013; 2013:5155–5158. [PubMed: 24110896]
23. Ding, Y., Chung, YC., Ying, L., Liang, D. Proc Intl Soc Mag Reson Med. Melbourne, Australia: 2012. Noise Behavior of DCE-MRI Reconstructions Using Compressed Sensing Based Method. abstract 2253
24. Ding Y, Chung YC, Simonetti OP. A method to assess spatially variant noise in dynamic MR image series. Magn Reson Med. 2010; 63(3):782–789. [PubMed: 20187185]
25. Dietrich O, Raya JG, Reeder SB, Reiser MF, Schoenberg SO. Measurement of signal-to-noise ratios in MR images: influence of multichannel coils, parallel imaging, and reconstruction filters. Journal of magnetic resonance imaging : JMRI. 2007; 26(2):375–385. [PubMed: 17622966]
26. Lin FH, Kwong KK, Belliveau JW, Wald LL. Parallel imaging reconstruction using automatic regularization. Magn Reson Med. 2004; 51(3):559–567. [PubMed: 15004798]
27. Sanchez-Gonzalez J, Tsao J, Dydak U, Desco M, Boesiger P, Paul Pruessmann K. Minimum-norm reconstruction for sensitivity-encoded magnetic resonance spectroscopic imaging. Magn Reson Med. 2006; 55(2):287–295. [PubMed: 16408281]
28. Sharma SD, Fong CL, Tzung BS, Law M, Nayak KS. Clinical image quality assessment of accelerated magnetic resonance neuroimaging using compressed sensing. Investigative radiology. 2013; 48(9):638–645. [PubMed: 23538890]
29. Lu W, Pauly KB, Gold GE, Pauly JM, Hargreaves BA. Slice encoding for metal artifact correction with noise reduction. Magnetic resonance in medicine : official journal of the Society of Magnetic Resonance in Medicine / Society of Magnetic Resonance in Medicine. 2011; 65(5):1352–1357.
30. Stevens KJ, Wallace CG, Chen W, Rosenberg JK, Gold GE. Imaging of the wrist at 1.5 Tesla using isotropic three-dimensional fast spin echo cube. Journal of magnetic resonance imaging : JMRI. 2011; 33(4):908–915. [PubMed: 21448957]
31. Stevens KJ, Busse RF, Han E, et al. Ankle: isotropic MR imaging with 3D-FSE-cube--initial experience in healthy volunteers. Radiology. 2008; 249(3):1026–1033. [PubMed: 19011194]
32. Ristow O, Stehling C, Krug R, et al. Isotropic 3-Dimensional Fast Spin Echo Imaging Versus Standard 2-Dimensional Imaging at 3.0 T of the Knee: Artificial Cartilage and Meniscal Lesions in a Porcine Model. Journal of computer assisted tomography. 2010; 34(2):260–269. [PubMed: 20351518]

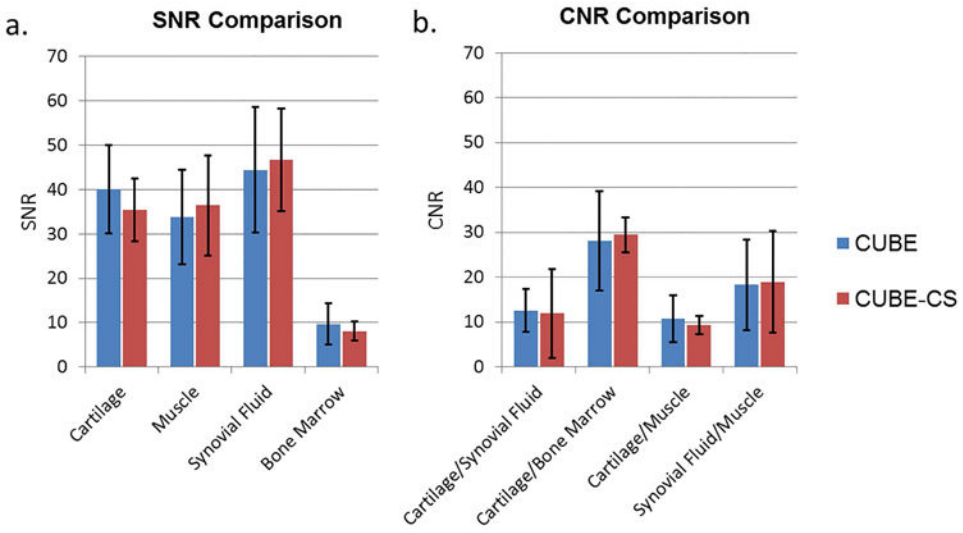

Figure 1.

(a) Mean and standard deviation of SNR of cartilage, muscle, synovial fluid, and bone marrow for CUBE and CUBE-CS. (b) Mean and standard deviation of CNR between cartilage and synovial fluid, cartilage and bone marrow, cartilage and muscle, and synovial fluid and muscle for CUBE and CUBE-CS.

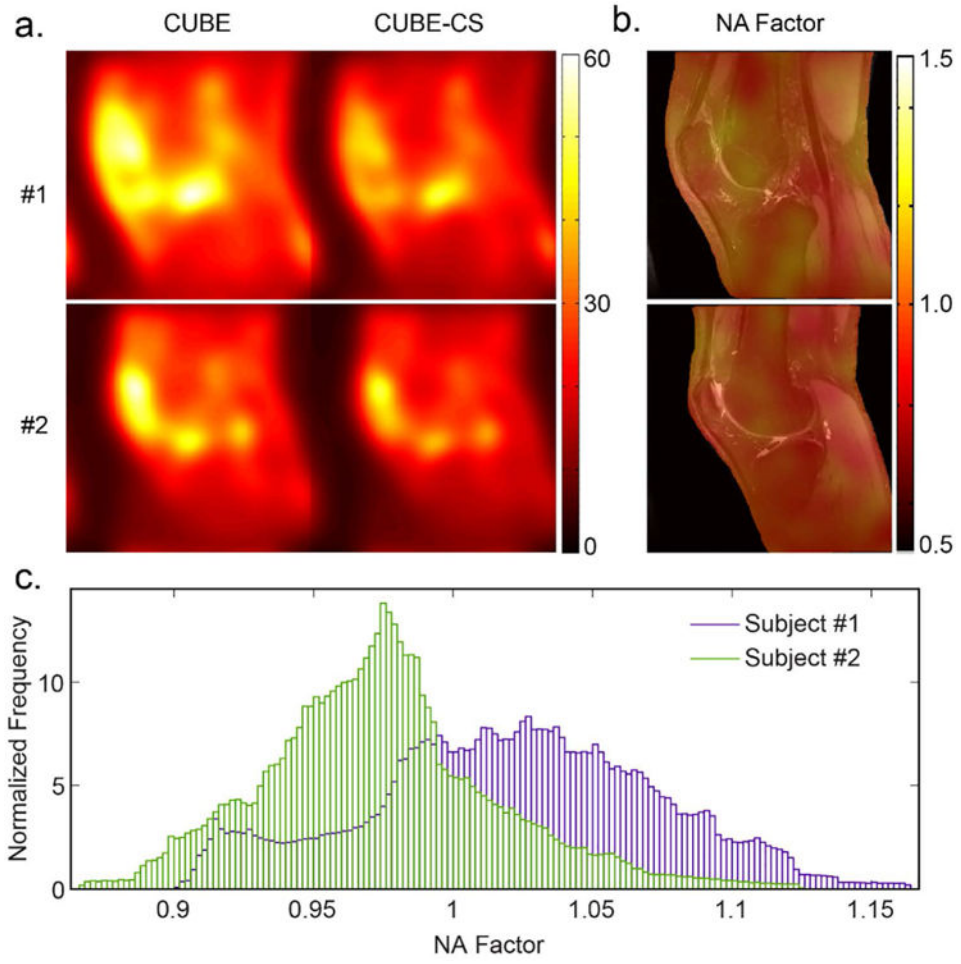

Figure 2.

(a) Estimated low frequency noise standard deviation maps for two healthy volunteers (#1 a central sagittal slice through the middle of the knee joint in a 30 year old male and #2 a sagittal slice through the lateral femoral condyle in a 29 year old female) for CUBE and CUBE-CS and corresponding (b) Color-coded noise amplification NA factor maps superimposed on top of the CUBE source image. (c) NA factor histograms show different noise amplification distribution for these two subjects but both histograms have mean value close to 1 indicating no noise amplification.

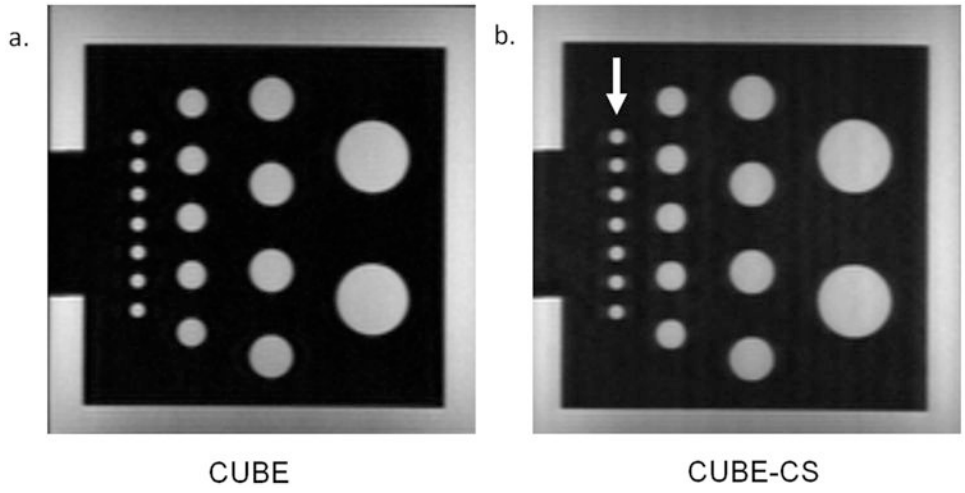

Figure 3.
(a and b) CUBE and CUBES images of a low resolution phantom with cylinders of diameters varying from 2mm to 12mm. Note image blurring on the CUBE-CS images (arrows) which did not result in a visible reduction in spatial resolution.

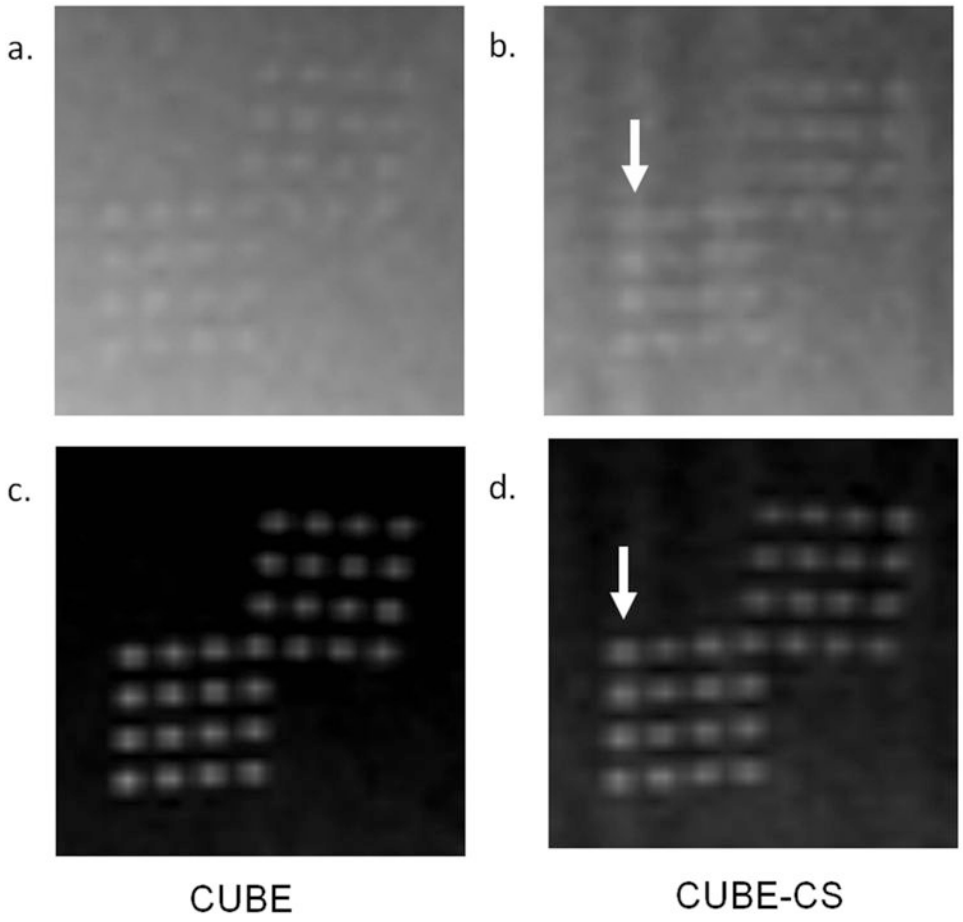

Figure 4.

CUBE and CUBES images of a 0.9mm high resolution, low contrast phantom (a and b) and 0.9mm high resolution, high contrast phantom (c and d). Note extensive image blurring on the CUBE-CS images (arrows) which resulted in a visible reduction in spatial resolution with apparent decrease in the distance between the dots in the phantoms. The decrease in spatial resolution was more prominent on the low contrast phantom than the high contrast phantom.

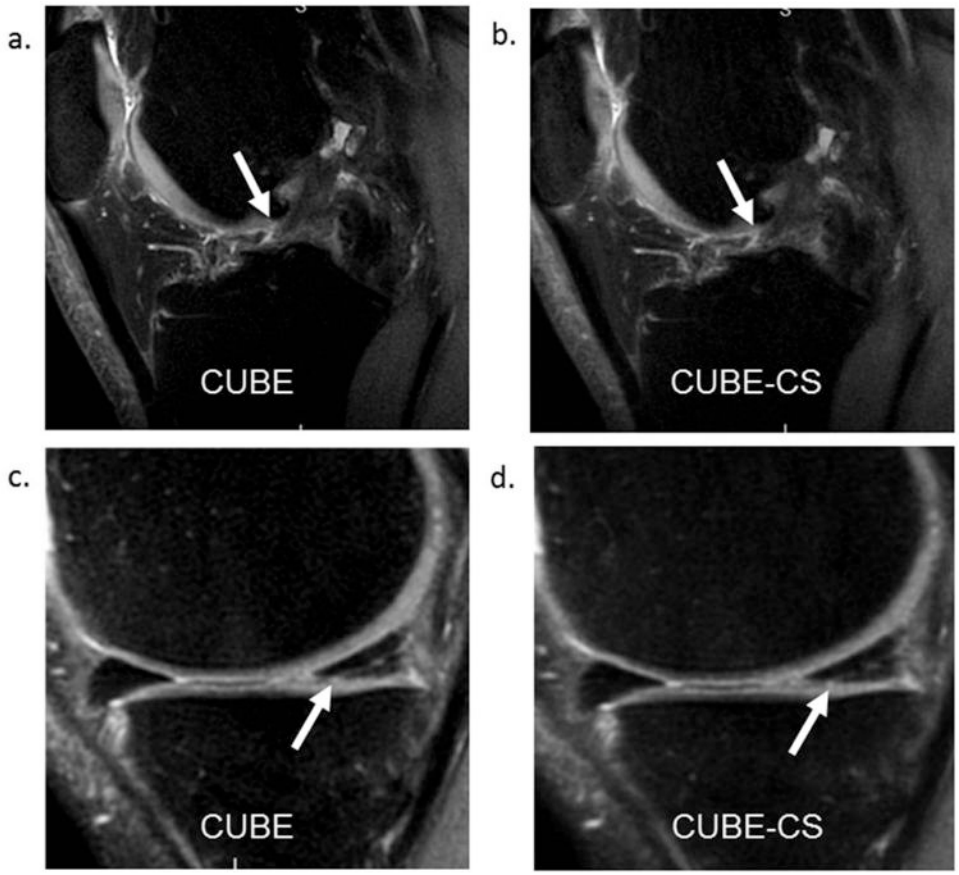

Figure 5.

(a and b) CUBE and CUBE-CS images in a 26 year old male show similar appearance of an anterior cruciate ligament tear (arrows). (c and d) CUBE and CUBE-CS images in a 46 year old female show similar appearance of a posterior horn medial meniscus tear (arrows).

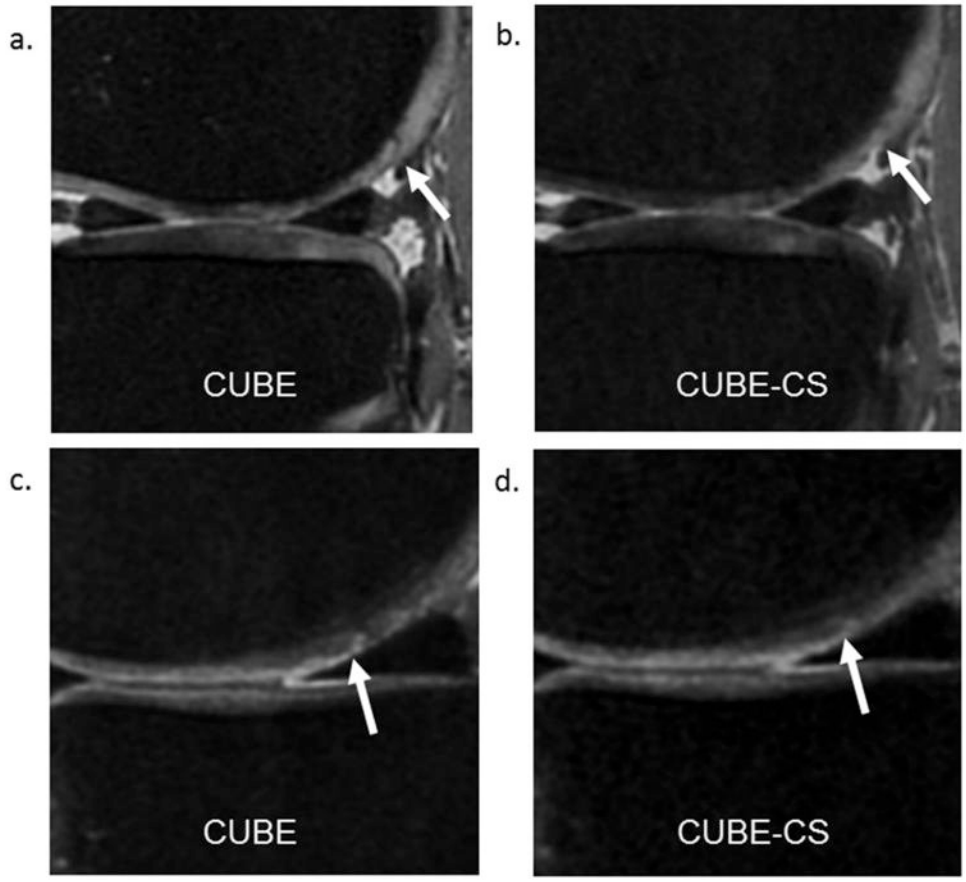

Figure 6.

(a and b) CUBE and CUBE-CS images in a 37 year old male show decreased conspicuity of a dark linear cartilage fissure on the posterior medial femoral condyle (arrows) on the CUBE-CS image due to increased image blurring. (c and d) CUBE and CUBE-CS images in a 41 year old female show decreased conspicuity of a superficial partial-thickness cartilage lesion on the central medial femoral condyle (arrows) on the CUBE-CS image due to increased image blurring.

Table 1

Kappa values with standard errors for agreement between the CUBE and CUBE-CS for detecting knee joint pathology for each radiologist

Knee Joint Pathology (Frequency)	Kappa Value (Standard Error)	
	Radiologist 1	Radiologist 2
Cartilage Lesion (N=159)	0.91 (0.02)	0.97 (0.02)
Bone Marrow Edema Lesion (N=62)	0.99 (0.01)	0.99 (0.01)
Medial Meniscus Tear (N=24)	1.00 (0.00)	1.00 (0.00)
Lateral Meniscus Tear (N=12)	1.00 (0.00)	1.00 (0.00)
Anterior Cruciate Ligament Tear (N=11)	1.00 (0.00)	1.00 (0.00)
Effusion (N=26)	1.00 (0.00)	1.00 (0.00)
Intra-Articular Body (N=13)	1.00 (0.00)	1.00 (0.00)

Frequency of knee joint pathology represents number of each joint abnormality detected by both radiologists on independent review of the CUBE and CUBE-CS images

Table 2

Kappa values with standard errors for agreement between the two radiologists for detecting knee joint pathology when using the CUBE and CUBE-CS

Knee Joint Pathology (Frequency)	Kappa Value (Standard Error)	
	CUBE	CUBE-CS
Cartilage Lesion (N=159)	0.82 (0.03)	0.85 (0.03)
Bone Marrow Edema Lesion (N=62)	0.87 (0.04)	0.87 (0.04)
Medial Meniscus Tear (N=24)	0.96 (0.04)	0.96 (0.04)
Lateral Meniscus Tear (N=12)	1.00 (0.00)	1.00 (0.00)
Anterior Cruciate Ligament Tear (N=11)	1.00 (0.00)	1.00 (0.00)
Effusion (N=26)	0.88 (0.07)	0.88 (0.07)
Intra-Articular Body (N=13)	0.84 (0.09)	0.88 (0.09)

Frequency of knee joint pathology represents number of each joint abnormality detected by both radiologists on independent review of the CUBE and CUBE-CS images

Table 3

Comparison of qualitative measures of image quality between CUBE and CUBE-CS for each radiologists

Measure of Image Quality	Grading Scale	Number of Patients	
		Radiologist 1	Radiologist 2
SNR	CUBE Slightly Better than CUBE-CS	3	3
	CUBE and CUBE-CS Identical	47	47
	CUBE-CS Slightly Better than CUBE	0	0
Tissue Contrast	CUBE Slightly Better than CUBE-CS	3	5
	CUBE and CUBE-CS Identical	47	45
	CUBE-CS Slightly Better than CUBE	0	0
Clarity of Cartilage	CUBE Slightly Better than CUBE-CS	25	22
	CUBE and CUBE-CS Identical	25	28
	CUBE-CS Slightly Better than CUBE	0	0
Clarity of Meniscus	CUBE Slightly Better than CUBE-CS	9	10
	CUBE and CUBE-CS Identical	41	40
	CUBE-CS Slightly Better than CUBE	0	0
Clarity of Tendon	CUBE Slightly Better than CUBE-CS	7	5
	CUBE and CUBE-CS Identical	43	45
	CUBE-CS Slightly Better than CUBE	0	0
Clarity of Muscle	CUBE Slightly Better than CUBE-CS	15	18
	CUBE and CUBE-CS Identical	35	32
	CUBE-CS Slightly Better than CUBE	0	0
Conspicuity of Knee Joint Pathology	CUBE Slightly Better than CUBE-CS	9	9
	CUBE and CUBE-CS Identical	41	41
	CUBE-CS Slightly Better than CUBE	0	0

No grades of CUBE significantly better than CUBE-CS or CUBE-CS significantly better than CUBE were given to any qualitative measure of image quality.